The Astrophysical Journal Letters, 825:L1 (5pp), 2016 July 1 doi:10.3847/2041-8205/825/1/L1

A STRINGENT LIMIT ON THE WARM DARK MATTER PARTICLE MASSES FROM THE ABUNDANCE OF $z = 6$ GALAXIES IN THE HUBBLE FRONTIER FIELDS

N. Menci[1], A. Grazian[1,2], M. Castellano[1], and N. G. Sanchez[3]
[1] INAF—Osservatorio Astronomico di Roma, via di Frascati 33, I-00040 Monte Porzio Catone, Italy
[2] Agenzia Spaziale Italiana Science Data Center, Via del Politecnico snc, I-00133, Roma, Italy
[3] Observatoire de Paris, LERMA, CNRS UMR 8112, 61, Observatoire de Paris PSL, Sorbonne Universités, UPMC Univ. Paris 6, 61 Avenue de l'Observatoire, F-75014 Paris, France
Received 2016 May 19; revised 2016 June 7; accepted 2016 June 8; published 2016 June 23

ABSTRACT

We show that the recently measured UV luminosity functions of ultra-faint lensed galaxies at $z \approx 6$ in the Hubble Frontier Fields provide an unprecedented probe for the mass m_X of the warm dark matter (WDM) candidates independent of baryonic physics. Comparing the measured abundance of the faintest galaxies with the maximum number density of dark matter halos in WDM cosmologies sets a robust limit of $m_X \geqslant 2.9$ keV for the mass of thermal relic WDM particles at a 1σ confidence level, $m_X \geqslant 2.4$ keV at 2σ, and $m_X \geqslant 2.1$ keV at 3σ. These constraints are *independent of the baryonic physics* involved in galaxy formation and constitute the tightest constraints on WDM particle mass derived to date. We discuss the impact of our results on the production mechanism of sterile neutrinos. In particular, if sterile neutrinos are responsible for the 3.5 keV line reported in observations of X-ray clusters, our results firmly rule out the Dodelson–Widrow production mechanism and yield $m_{\rm sterile} \gtrsim 6.1$ keV for sterile neutrinos produced via the Shi–Fuller mechanism.

Key words: dark matter – galaxies: abundances – galaxies: formation

1. INTRODUCTION

In recent years, impressive improvement in the measurement of the faint end (down to UV magnitudes $M_{\rm UV} \approx -16$) of the galaxy luminosity function (LF) at high redshift $z \gtrsim 6$ has been made possible by the Wide Field Camera 3 on the *Hubble Space Telescope* (*HST*) (see, e.g., Bouwens et al. 2011, 2015; McLure et al. 2013; Finkelstein et al. 2015). With the Hubble Frontier Fields (HFF) program, even fainter galaxies, with intrinsic magnitudes below the *HST* limits, can be detected thanks to magnification by foreground galaxy clusters. The HFF program has enabled the detection of galaxies with $M_{\rm UV} \approx -15$ at $z \approx 6$ (Atek et al. 2015; Ishigaki et al. 2015) or $M_{\rm UV} \leqslant -17$ at $z \approx 8$ (Atek et al. 2015; Ishigaki et al. 2015; Laporte et al. 2015; Castellano et al. 2016a)

Recently, the observations of lensed background galaxies in Abell 2744 and MACS 0416 were used to measure the LF of galaxies down to ultra-faint magnitudes $M_{\rm UV} = -12.5$ at $z \approx 6$ (Livermore et al. 2016, hereafter LFL16). Such measurements have been shown to provide important constraints on the contribution to reionization, and on the star formation and feedback processes of primeval galaxies (Castellano et al. 2016b). However, their potential implication for constraining alternative dark matter (DM) models has not been pointed out yet.

In particular, the observed high density of galaxies measured at $z \approx 6$ has a deep impact on warm dark matter (WDM; see Bode et al. 2001) models of galaxy formation, based on DM candidates with masses in the keV scale (de Vega & Sanchez 2010). In these models, the population of low-mass galaxies is characterized by lower abundances and shallower central density profiles compared to cold dark matter (CDM) due to the dissipation of small-scale density perturbations produced by the free streaming of the lighter and faster DM particles. Thus, WDM scenarios have been proposed as a solution to some unsolved issues affecting the CDM model on small scales $\lesssim$1 Mpc, like the steepness of the density profiles in the inner regions of dwarf galaxies (see de Vega et al. 2014) and the overabundance of faint dwarfs around our Galaxy and in our Local Group (see, e.g., Lovell et al. 2012), as well as in the field (Menci et al. 2012; see also Macció et al. 2012; Papastergis et al. 2015). Indeed, while a refined treatment of baryonic effects entering galaxy formation (in particular feedback from supernovae) can contribute to solving the problems (see, e.g., Governato et al. 2012; Di Cintio et al. 2014), feedback effects can hardly explain the excess of massive satellite DM halos with virial velocities $V_{\rm vir} \geqslant 20\,{\rm km\,s^{-1}}$ relative to the number of observed bright dwarf galaxies (Boylan-Kolchin et al. 2012) and—most of all—the overprediction of the abundance of field dwarfs with $V_{\rm vir} \approx 40$–$60\,{\rm km\,s^{-1}}$ (Klypin et al. 2015).

The effect of assuming WDM on galaxy formation strongly depends on the mass of the candidate DM particle (see, e.g., Polisensky & Ricotti 2011; Lovell et al. 2012; Macció et al. 2012; Schneider et al. 2012). In fact, the mass of the DM particle determines the suppression of the density power spectrum compared to the CDM case, which drives the formation of cosmic structures. The half-mode mass $M_{\rm hm}$—determining the mass scale at which the WDM spectrum is suppressed by 1/2 compared to CDM—is a strong inverse function of the WDM particle mass. Thus, different WDM power spectra are generally labeled in terms of the mass m_X of WDM thermal relic particles, for which a one-to-one correspondence exists between the power spectrum and the particle mass.

Existing astrophysical bounds on the thermal relic mass m_X have been set by different authors (e.g., $m_X \geqslant 2.3$ keV, Polisensky & Ricotti 2011; $m_X \gtrsim 1.5$ keV, Lovell et al. 2012; Horiuchi et al. 2014; $m_X \geqslant 2$ keV, Kennedy et al. 2014) by comparing the predictions from *N*-body WDM simulations or semianalytic models with the abundance of observed ultra-faint satellites. Note, however, that the latter are appreciably sensitive to the assumed completeness corrections (see

discussions in Abazajian et al. 2011; Schultz et al. 2014). At higher redshifts ($z \approx 6$) a limit of $m_X \gtrsim 1$ keV has been derived from the UV LFs of faint galaxies ($M_{UV} \approx -16$) by Schultz et al. (2014). Since these approaches are based on the comparison between observed LFs and predicted mass function of DM halos in different WDM models, the delicate issue in these methods is their dependence on the physics of baryons determining the mass-to-light ratio of faint galaxies. Although, to a lesser extent, uncertainties in the baryonic physics also affect (see Garzilli & Boyarsky 2015 and the discussion in Viel et al. 2013) the tighter constraints achieved so far for $m_X \geqslant 3$ keV, derived by comparing the small-scale structure in the Lyα forest of high-resolution ($z > 4$) quasar spectra with hydrodynamical N-body simulations (Viel et al. 2013).

An effective way of bypassing the physics of baryons can be found by exploiting the downturn of the halo mass distribution $\phi(M, z)$ in WDM cosmology at masses close to the half-mode mass scale M_{hm} (see Schneider et al. 2012, 2013; Angulo et al. 2013; Benson et al. 2013; Pacucci et al. 2013). At any given redshift, the corresponding maximum number density of halos $\overline{\phi_{m_X}(z)} \approx \phi(M_{hm}(m_X), z)$ increases with the WDM particle mass (determining the half-mode mass). Thus, measuring galaxy abundances larger than $\overline{\phi_{m_X}(z)}$ at a given redshift sets a lower limit on m_X which is *completely independent* of the physics of the baryons, since any baryonic effect can only decrease the number of luminous galaxies compared to the number of host DM halos. Such a method is limited by the depth required to measure large galaxy number densities; in fact, such high densities are more easily attained at the faint end of high-redshift LFs.

Pacucci et al. (2013) have applied the above procedure to the number density corresponding to two galaxies detected at $z \approx 10$ by the Cluster Lensing And Supernova survey with Hubble obtaining a lower limit $m_X \geqslant 0.9$ keV (2σ). A similar limit has been obtained by Lapi & Danese (2015) from existing deep UV LFs at $z \approx 7$. A different strategy has been adopted by Menci et al. (2016), who used abundances obtained at lower $z \approx 2$ from UV LFs of galaxies lensed by the nearby cluster A1689. The ultra-faint magnitudes $M_{UV} \approx -13$ reached by the observed sample allows us to obtain a lower bound $m_X \geqslant 1.5$ keV, which is again independent of baryon physics.

Obtaining tighter limits on m_X with the above method requires reaching faint magnitudes ≈ -14 at high redshifts $z \gtrsim 6$. Thus, the recent measurements of the UV LFs of lensed galaxies down to ultra-faint magnitudes $M_{UV} = -12.5$ at $z \approx 6$ by LFL16 constitute an unprecedented opportunity to derive *strong* constraints on the WDM particle mass m_X that are independent of baryonic physics.

2. THE MASS FUNCTION OF HALOS IN WDM COSMOLOGIES

The computation of the halo mass function in WDM models is based on the standard procedure described and tested against N-body simulations in Schneider et al. (2012, 2013), Benson et al. (2013), and Angulo et al. (2013); our computation has been tested against simulations in Menci et al. (2016). Here, we provide a brief outline of the main steps.

The key quantity entering the mass function is the variance of the linear power spectrum $P(k)$ of DM perturbations (in terms of the wavenumber $k = 2\pi/r$). Its dependence on the spatial scale r of perturbations is

$$\frac{d \log \sigma^2}{d \log r} = -\frac{1}{2\,\pi^2\,\sigma^2(r)}\,\frac{P(1/r)}{r^3}. \quad (1)$$

Here, we have used a sharp-k form (a top-hat sphere in Fourier space) for the window function $W(kr)$ relating the variance to the power spectrum $\sigma^2(M) = \int dk\; k^2\; P(k) W(kr) / 2\,\pi^2$.

Indeed, in the case of WDM spectra $P(k)$ suppressed at small scales with respect to the scale-invariant CDM behavior, both theoretical arguments (Benson et al. 2013; Schneider et al. 2013) and comparisons with N-body simulations (see the authors above and Angulo et al. 2013) impose a sharp-k form (a top-hat sphere in Fourier space) for the window function. In fact, a top-hat filter in the real space would result into diverging mass functions for small scales despite the small-scale suppression in the power spectrum, due to the fact that longer wavelength modes are getting re-weighted as the mass scale of the filter increases. However, for a sharp-k filter, the normalization c entering the relation between the halo mass $M = 4\pi\,\overline{\rho}\,(cr)^3/3$, and the filter scale r must be calibrated through simulations (here, $\overline{\rho}$ is the background density of the universe). All studies in the literature yield values for c in the range $c = 2.5$–2.7 (see, e.g., Angulo et al. 2013; Benson et al. 2013; Schneider et al. 2013). We shall consider the effect of such an uncertainty on our results.

In WDM scenarios, the spectrum P_{WDM} is suppressed with respect to the CDM case P_{CDM} below a characteristic scale depending on the mass m_X of the WDM particles. If WDM is composed of relic thermalized particles, the suppression factor can be parametrized as (Bode et al. 2001)

$$\frac{P_{WDM}(k)}{P_{CDM}(k)} = [1 + (\alpha\,k)^{2\,\mu}]^{-10/\mu}. \quad (2)$$

Here, the WDM free-streaming scale enters through the quantity

$$\alpha = 0.049\left[\frac{\Omega_X}{0.25}\right]^{0.11}\left[\frac{m_X}{\mathrm{keV}}\right]^{-1.11}\left[\frac{h}{0.7}\right]^{1.22}\frac{h^{-1}}{\mathrm{Mpc}}, \quad (3)$$

depending on the WDM particle mass. Here, Ω_X is the WDM density parameter, h is the Hubble constant in units of $100\,\mathrm{km\,s^{-1}\,Mpc^{-1}}$, and $\mu = 1.12$. A similar expression holds for sterile neutrinos provided one substitutes the mass m_X with a mass $m_{sterile}$ adopting proper conversion factors (depending on the assumed neutrino production mechanisms; see, e.g., Destri et al. 2013). Note that the expressions in Equations (2) and (3) represent fitting formulae for the actual power spectra of thermal relic WDM obtained through the CAMB (Lewis et al. 2000) or the CMBFAST (Seljak & Zaldarriaga 1996) Boltzmann solver in the case of thermal relics. The difference between the actual Boltzmann solutions and the fitting formulas in Equations (2) and (3) is at the percent level (see, e.g., Lovell et al. 2015), with differences in the quantities α and μ estimated by different authors that are below 5% (see, e.g., Hansen et al. 2002; Viel et al. 2005). A fitting formula providing an even better agreement with the true numerical solutions has been presented in Destri et al. (2013), although it deviates from the form in Equations (2) and (3) by at most 3%. In our results, we will incorporate the above uncertainties,

which also enter into the expression for the half-mode mass given below in Equation (5).

The differential halo mass function (per unit log M) based on the extended Press & Schechter approach (Bond et al. 1991; Benson et al. 2013; Schneider et al. 2013) reads

$$\frac{d\,\phi}{d\,\log M} = \frac{1}{6}\,\frac{\overline{\rho}}{M} f(\nu) \frac{d\,\log \sigma^2}{d\,\log r}. \quad (4)$$

Here, $\nu \equiv \delta_c^2(t)/\sigma^2$ depends on the linearly extrapolated density for collapse in the spherical model $\delta_c = 1.686/D(t)$, and $D(t)$ is the growth factor of DM perturbations. We conservatively assume a spherical collapse model for which $f(\nu) = \sqrt{2\nu/\pi}\,\exp(-\nu/2)$. Assuming an ellipsoidal collapse model would yield lower halo mass function at the low-mass end and—hence—even tighter constraints on the WDM particle mass. To adopt a conservative approach, we do not include the effect of residual thermal velocities; in fact, as shown by Benson et al. (2013), this would lead to an increase of the collapse threshold δ_c at scales below the free-streaming scale resulting in even tighter constraints on m_X.

The mass function in Equation (4) is computed after substituting Equation (1), with a power spectrum $P(k) = P_{WDM}(k)$ determined by the WDM particle mass m_X after Equations (2)–(3) (for P_{CDM} we adopt the form by Bardeen et al. 1986). The resulting mass functions are characterized by a maximum value at masses close to the "half-mode" mass (see Benson et al. 2013; Schneider et al. 2012, 2013; Angulo et al. 2013; Menci et al. 2016)

$$M_{hm} = \frac{4\pi}{3}\,\overline{\rho}\left[\pi\alpha\,(2^{\mu/5}-1)^{-\frac{1}{2\mu}}\right]^3. \quad (5)$$

Correspondingly, the cumulative mass functions saturate to a maximum value $\overline{\phi_{m_X}(z)} \approx \phi(M_{hm}(m_X), z)$. The dependence of the scale α (Equation (3)) on the WDM particle mass m_X yields a half-mode mass ranging from $M_{hm} \approx 10^{10}\,M_\odot$ for $m_X = 1$ keV to $M_{hm} \approx 10^8\,M_\odot$ for $m_X = 4$ keV.

3. RESULTS

In Figure 1, we show the cumulative mass function $\phi(>M)$ computed from Equation (4) at $z = 6$ for different assumed WDM particle masses, adopting recent Planck cosmological parameters: $\Omega_m = 0.32$, $\Omega_\Lambda = 0.68$, $\Omega_b = 0.05$, $h = 0.7$, $\sigma_8 = 0.83$. All the mass functions saturate to a maximum number density $\overline{\phi}_{m_X} \approx \phi(M_{hm})$. This is compared with the observed number density ϕ_{obs} of galaxies with $M_{UV} \leqslant -12.5$ corresponding to the LFL16 LFs at $z = 6$ within 1σ, 2σ, and 3σ (shaded areas). In order to derive the observed cumulative number density ϕ_{obs} (and its confidence levels) corresponding to the differential LFs $\Phi(M_{UV})$ of LFL16, we have used the values shown in their Figure 10 with the corresponding 1σ uncertainties in each magnitude bin. We produced Monte Carlo simulations by extracting random values $\Phi_{random}(M_{UV})$ of the LF in each magnitude bin according to a Gaussian distribution with variance given by the error bar in LFL16. Thus, for each simulation we produced a new realization of the $z = 6$ LF. From this, a cumulative number density ϕ_{random} has been derived by summing up the values of $\Phi_{random}(M_{UV})$ in all the observed magnitude bins in the range $-22.5 \leqslant M_{UV} \leqslant -12.5$. We carried out $N_{sim} = 10^7$ simulations to compute the probability distribution function (PDF) of the cumulative number density ϕ_{random}. We obtain a median value $\log \phi_{obs}/\mathrm{Mpc}^3 = 0.54$, while from the relevant percentiles of the PDF we derive lower bounds 0.26, 0.01, and -0.32 at the 1σ, 2σ, and 3σ confidence levels, respectively. We have checked that the median value of the differential LF Φ_{random} obtained from our simulations is consistent (within 3%) with the best-fit value of the LFL16 LF.

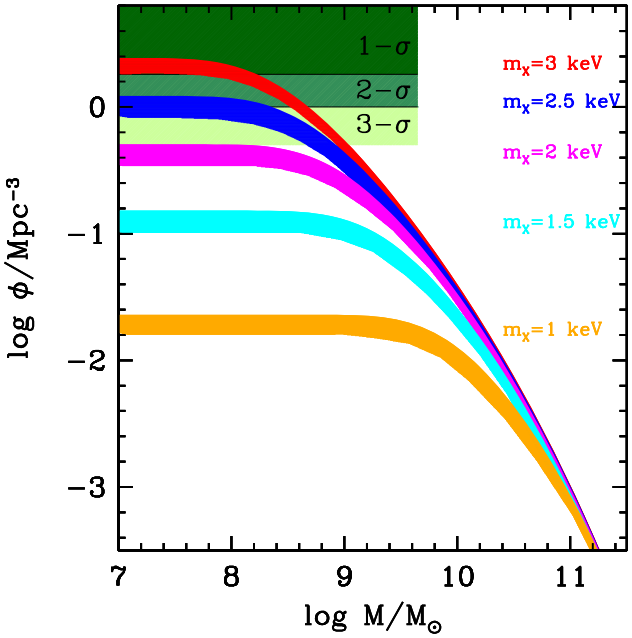

Figure 1. Cumulative mass functions computed at $z = 6$ for different values of the WDM particle mass m_X shown by the labels on the right. The thickness of the lines represent the uncertainties in the theoretical predictions related to the window function and to the adopted fitting formula for the WDM power spectrum discussed in Section 2. The shaded areas correspond to the observed number density of galaxies with $M_{UV} \leqslant -12.5$ within the 1σ, 2σ, and 3σ confidence levels.

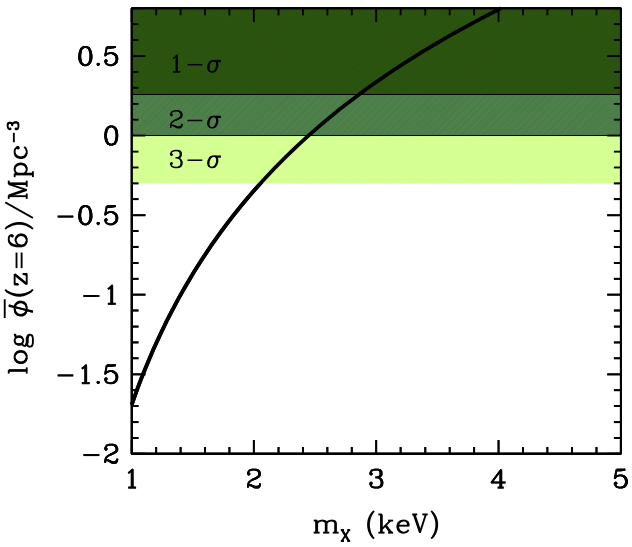

Figure 2. For different values of the thermal relic mass m_X, we show the maximum value (including the theoretical uncertainties) of the predicted number density of DM halos ϕ at $z = 6$. The shaded areas represent the observed number density of galaxies with $M_{UV} \leqslant -12.5$ within the 1σ, 2σ, and 3σ confidence levels.

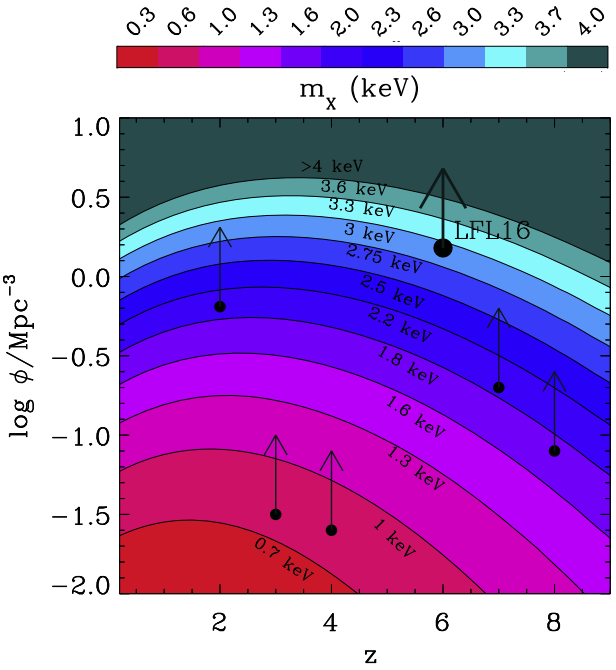

Figure 3. Contours show the maximum number density of DM halos (*y*-axis) obtained at different redshifts (*x*-axis) assuming different values for the WDM particle mass m_X (contour levels and colors). Such abundances are compared with the lower limit (at the 1σ level) set by the different UV galaxy LFs in the literature integrated down to their faintest magnitude bin at $z = 2$ (Alavi et al. 2014), at $z = 3 - 4$ (Parsa et al. 2016), and at $z > 6$ by LFL16. The thick dot and error bar correspond to the UV LFs measured by LFL16 at $z = 6$, which provide the tightest bound on m_X.

In Figure 2, we compare ϕ_{obs} and $\overline{\phi}_{m_X}$ as a function of m_X. Since luminous galaxies cannot outnumber DM halos, the condition $\phi_{obs} \leqslant \overline{\phi}_{m_X}$ yields $m_X \gtrsim 2.9$ keV at the 1σ level, $m_X \geqslant 2.4$ keV at the 2σ level, and $m_X \geqslant 2.1$ keV at the 3σ level. Our constraints are the tightest derived so far from galaxy counts. Although these constraints are less stringent than the 2σ limit $m_X \geqslant 3.3$ keV derived from the Lyα forest (Viel et al. 2013), our limits are *entirely independent* of the modeling of baryons physics that affects the constraints from the Lyα absorbers.

The method we have applied is similar to that adopted by Pacucci et al. (2013) at $z = 10$, by Lapi & Danese (2015) at $z \approx 7$, and by Menci et al. (2016) at $z \approx 2$. Compared to such works, we derive significantly tighter constraints on m_X due to the unprecedented depth reached by the LF measurements in LFL16. To provide a comparison with previous results and to show how the LFL16 measurements made it possible to significantly improve the constraint on m_X, we show in Figure 3 the thermal relic mass m_X that can be probed by observing a given number density of galaxies $\overline{\phi}_{m_X}$ (in the *y*-axis) at different redshifts (*x*-axis). Such values are compared with the lower bounds set by different measurements at various redshifts. Thus, the contour corresponding to the lower tip of the arrow defines the mass m_X probed by the corresponding observations (at the 1σ level). Our 1σ lower bound derived from LFL16 is shown by the large circle at $z = 6$ and provides the most stringent limit derived so far.

4. CONCLUSIONS

We show that the recently measured UV LFs of ultra-faint lensed galaxies at $z \approx 6$ provide unprecedentedly strong constraints on the mass of WDM candidates m_X, which is independent of baryonic physics. Comparing with the measured abundance of the faintest galaxies with the maximum number density of DM halos in WDM cosmologies sets a robust limit $m_X \geqslant 2.9$ keV for the mass of thermal relic WDM particles at the 1σ confidence level and $m_X \geqslant 2.4$ keV at the 2σ level.

The corresponding lower limit for the sterile neutrino mass depends on the production model. Accurate conversion factors relating the thermal relic mass m_X to the values of $m_{sterile}$ giving the same power spectrum are provided by Destri et al. (2013), together with a discussion on the accuracy and comparison of the conversion factors in the literature. They obtain $m_{sterile} \simeq 2.85\,\mathrm{keV}\ (m_X/\mathrm{keV})^{4/3}$ for the Dodelson & Widrow (1994) mechanism, $m_{sterile} \simeq 2.55\, m_X$ for the Shi & Fuller (1999) resonant production (for vanishing lepton asymmetry), and $m_{sterile} \simeq 1.9\, m_X$ for the neutrino Minimal Standard Model (Shaposhnikov & Tkachev 2006).

If sterile neutrinos with mass $m_{sterile} \approx 7$ keV are responsible for the recent unidentified X-ray line at 3.5 keV reported in observations of X-ray clusters (Bulbul et al. 2014; Boyarsky et al. 2014), our 2σ constraint $m_X \geqslant 2.4$ keV firmly rules out—independently of astrophysical modeling and of incompleteness corrections—the Dodelson–Widrow mechanism for the production of sterile neutrinos, already disfavored by previous results (see Horiuchi et al. 2014).

While our results are robust with respect to astrophysical modeling of baryonic processes involved in galaxy formation, they rely on the observed LFs in LFL16. Such measurements indeed exploit state-of-the-art analyses of the space densities of ultra-faint star-forming galaxies at $z \geqslant 6$, thanks to the very faint limits ($M_{UV} = -12.5$ at $z = 6$) reached by deep *HST* observations by exploiting the strong lensing magnifications (of a factor of 50 or more) of the clusters in the HFF campaign. This effect makes it possible to reach luminosities that are more than a factor of 100 deeper than the ones available in unlensed *HST* pointings. The strong lensing magnifications have been derived by adopting the full range of possible lens models produced for the HFF by seven independent groups who used different assumptions and methodologies, to check the systematic effects of different lens models on the LFs. Notably, LFL16 concluded that the logarithmic slope at faint end varies by less than 4% using the different lensing maps available, without any turnover down to $M_{UV} = -12.5$ at $z = 6$. As for the statistics, we note that the large number of galaxies investigated (167 galaxies at $z = 6$) and the availability of two independent lines of sight also allow LFL16 to reduce the cosmic variance effect, which usually affects the measurements of the LFs at these high redshifts.

However, the results in LFL16 can still be improved both in accuracy and statistics: first, through refined methods to assemble the final source catalog, which is now obtained by a simple positional cross-matching of 22 independent catalogs derived from different wavelet images in various bands; second, by reducing the uncertainty on the photometric redshifts that, as stated in LFL16, dominates over the variance of different lens models, except in cases where the magnification is high ($\geqslant$10). In this respect, the combination of different photometric redshift estimates (e.g., Castellano et al. 2016a) can be a promising way to further reduce the uncertainties on the LF.

In the future, the current results can be further improved by extending the present analysis to all six Frontier Field clusters (see Lotz et al. 2016). This will make it possible to reduce the error bars on the LF at high-z, thanks to the larger number statistics (450 galaxies at $z \sim 6$ are expected) and to the reduced cosmic variance thanks to six independent lines of sights.

We warmly thank Anna Nierenberg for substantial help in improving the manuscript.

REFERENCES

Abazajian, K. N., Calabrese, E., Cooray, A., et al. 2011, APh, 35, 177
Alavi, A., Siana, B., Richard, J., et al. 2014, ApJ, 780, 143
Angulo, R. E., Hahn, O., & Abel, T. 2013, MNRAS, 434, 3337
Atek, H., Richard, J., Kneib, J.-P., et al. 2015, ApJ, 800, 18
Bardeen, J. M., Bond, J. R., Kaiser, N., & Szalay, A. S. 1986, ApJ, 304, 15
Benson, A. J., Farahi, A., Cole, S., et al. 2013, MNRAS, 428, 1774
Bode, P., Ostriker, J. P., & Turok, N. 2001, ApJ, 556, 93
Bond, J. R., Cole, S., Efstathiou, G., & Kaiser, N. 1991, ApJ, 379, 440
Bouwens, R. J., Illingworth, G. D., Oesch, P. A., et al. 2011, ApJ, 737, 90
Bouwens, R. J., Illingworth, G. D., Oesch, P. A., et al. 2015, ApJ, 803, 34
Boyarsky, A., Ruchayskiy, O., Iakubovskyi, D., & Franse, J. 2014, PhRvL, 113, 251301
Boylan-Kolchin, M., Bullock, J., & Kaplinghat, M. 2012, MNRAS, 415, L40
Bulbul, E., Markevitch, M., Foster, A. R., et al. 2014, ApJ, 789, 13
Castellano, M., Amorin, R., Merlin, E., et al. 2016a, A&A, 590A, 31
Castellano, M., Yue, B., Ferrara, A., et al. 2016b, ApJL, in press (arXiv:1605.01524)
de Vega, H. J., Salucci, P., & Sanchez, N. G. 2014, MNRAS, 442, 2717
de Vega, H. J., & Sanchez, N. G. 2010, MNRAS, 404, 885
Destri, C., de Vega, P., & Sanchez, N. G. 2013, PhRvD, 88, 083512
Di Cintio, A., Brook, C. B., Dutton, A. A., et al. 2014, MNRAS, 441, 2986
Dodelson, S., & Widrow, L. M. 1994, PhRvL, 72, 17
Finkelstein, S. L., Ryan, R. E. J., Papovich, C., et al. 2015, ApJ, 810, 71
Garzilli, A., & Boyarsky, A. 2015, arXiv:1510.07006v1
Governato, F., Zolotov, A., Pontzen, A., et al. 2012, MNRAS, 422, 1231
Hansen, S. H., Lesgourgues, J., Pastor, S., & Silk, J. 2002, MNRAS, 333, 544
Horiuchi, S., Humphrey, P. J., Onorbe, J., et al. 2014, PhRvD, 89, 5017
Ishigaki, M., Kawamata, R., Ouchi, M., et al. 2015, ApJ, 799, 12
Kennedy, R., Frenk, C. S., Cole, S., & Benson, A. 2014, MNRAS, 442, 2487
Klypin, A., Karachentsev, I., Makarov, D., & Nasonova, O. 2015, MNRAS, 454, 1798
Lapi, A., & Danese, L. 2015, JCAP, 09, 003
Laporte, N., Streblyanska, A., Kim, S., et al. 2015, A&A, 575, A92
Lewis, A., Challinor, A., & Lasenby, A. 2000, ApJ, 538, 473
Livermore, R. C., Finkelstein, S. L., & Lotz, J. M. 2016, arXiv:1604.06799
Lotz, J. M., Koekemoer, A., Coe, D., et al. 2016, ApJ, submitted (arXiv:1605.06567)
Lovell, M. R., Bose, S., Boyarsky, A., et al. 2015, MNRAS, submitted (arXiv:1511.04078)
Lovell, M. R., Eke, V., Frenk, C. S., et al. 2012, MNRAS, 420, 2318
Macció, A., Paduroiu, S., Anderhalden, D., Schneider, A., & Moore, B. 2012, MNRAS, 424, 1105
McLure, R. J., Dunlop, J. S., Bowler, R. A. A., et al. 2013, MNRAS, 432, 2696
Menci, N., Fiore, F., & Lamastra, A. 2012, MNRAS, 421, 2384
Menci, N., Sanchez, N. G., Castellano, M., & Grazian, A. 2016, ApJ, 818, 90
Pacucci, F., Mesinger, A., & Haiman, Z. 2013, MNRAS, 435, L53
Papastergis, E., Giovanelli, R., Haynes, M. P., & Shankar, F. 2015, A&A, 575, A113
Parsa, S., Dunlop, J. S., McLure, R. J., & Mortlock, A. 2016, MNRAS, 456, 3194
Polisensky, E., & Ricotti, M. 2011, PhRvD, 83, 3506
Schneider, A., Smith, R. E., Maccio', A. V., & Moore, B. 2012, MNRAS, 424, 684
Schneider, A., Smith, R. E., & Reed, D. 2013, MNRAS, 433, 1573
Schultz, C., On orbe, J., Abazajian, K. N., & Bullock, J. S. 2014, MNRAS, 442
Seljak, U., & Zaldarriaga, M. 1996, ApJ, 469, 437
Shaposhnikov, M., & Tkachev, I. 2006, PhLB, 639, 414
Shi, X. d., & Fuller, G. M. 1999, PhRvL, 82, 2832
Viel, M., Becker, G. D., Bolton, J. S., & Haehnelt, M. G. A. 2013, PhRvD, 88, 3502
Viel, M., Lesgourgues, J., Haehnelt, M. G., Matarrese, S., & Riotto, A. 2005, PhRvD, 71, 063534